

# Multi-time quantum process tomography on a superconducting qubit

Christina Giarmatzi,<sup>1,2,\*</sup> Tyler Jones,<sup>2,3,4,\*</sup> Alexei Gilchrist,<sup>2,5</sup>  
Prasanna Pakkiam,<sup>2,3</sup> Arkady Fedorov,<sup>2,3</sup> and Fabio Costa<sup>3,6</sup>

<sup>1</sup>*School of Computer Science, University of Technology Sydney,  
Ultimo, Sydney, New South Wales 2007, Australia*

<sup>2</sup>*ARC Centre of Excellence for Engineered Quantum Systems,  
St. Lucia, Brisbane, Queensland 4072, Australia*

<sup>3</sup>*School of Maths and Physics, University of Queensland,  
St. Lucia, Brisbane, Queensland 4072, Australia*

<sup>4</sup>*Fiasqo, Brisbane, Queensland 4072, Australia*

<sup>5</sup>*School of Mathematical and Physical Sciences, Macquarie University, Sydney, New South Wales 2122, Australia*

<sup>6</sup>*Nordita, Stockholm University and KTH Royal Institute of Technology, Stockholm, 106 91, Sweden*

Current quantum technologies are at the cusp of becoming useful, but still face formidable obstacles such as noise. Noise severely limits the ability to scale quantum devices to the point that they would offer an advantage over classical devices. To understand the sources of noise it is necessary to fully characterise the quantum processes occurring across many time steps; only this would reveal any time-correlated noise called non-Markovian. Previous efforts have attempted such a characterisation but obtained only a limited reconstruction of such multi-time processes. In this work, we fully characterise a multi-time quantum process on superconducting hardware using in-house and cloud-based quantum processors. We achieve this by employing sequential measure-and-prepare operations combined with post-processing. Employing a recently developed formalism for multi-time processes, we detect general multi-time correlated noise. We also detect quantum correlated noise which demonstrates that part of the noise originates from quantum sources, such as physically nearby qubits on the chip. Our findings and techniques are expected to advance error-mitigation techniques in current quantum hardware, a necessary component to scale up the technology and achieve its true potential.

## I. INTRODUCTION

The characterisation of noise is a critical requirement for the advancement of quantum technologies. Noise is present in all current quantum devices as they interact with their environment; for many devices, this includes non-Markovian noise due to temporal correlations across a multi-time process. While most current techniques assume Markovian noise, this assumption fails in realistic quantum devices and non-Markovian noise has been reported in state-of-the-art quantum computing devices (such as IBM and Google) [1–3].

Past general approaches to capture non-Markovian noise only provide access to two times of a quantum process through dynamical maps [4–10]. Beyond this, a number of techniques designed to reduce non-Markovian noise have been developed [11–15], and shown to increase computational accuracy [11], but all rely on ad-hoc methods, and a rigorous approach is still lacking.

Recently, a formalism was developed that constructs a *process matrix* [16, 17], which encodes all multi-time correlations in a quantum process. In this formalism, non-Markovian noise is rigorously captured and can be further investigated in terms of its nature (quantum or classical) and amount [18, 19], as well as memory length

and location in the device [20] with a prospect of scalability [21] and extending current characterisation methods to non-Markovian regimes [22]. The approach has been used in distinct experimental scenarios, successfully detecting non-Markovian noise [1, 20, 23–27].

However, full reconstruction of a multi-time process matrix requires implementing sequentially informationally-complete operations, such as measure-and-prepare, on the system at *every* time step. Based on the assumption that this procedure requires mid-circuit measurements with a fast feed-forward of signal—unavailable in current quantum computing platforms—previous work did not succeed in performing full tomography but rather achieved a partial characterisation of non-Markovian noise, for example through a ‘restricted’ process matrix [27–30].

Here, we present the first implementation of a rigorous and complete description of non-Markovian noise on quantum devices with superconducting qubits. We achieve this through full process tomography of a multi-time quantum process and obtain measures of non-Markovianity. We implement mid-circuit measurements and overcome the need for a feed-forward mechanism with a post-processing trick. We use devices from the labs of the University of Queensland and the cloud capabilities of IBM Quantum [31]. We measure general and quantum non-Markovian noise in all cases and build a theoretical model to compare our findings. Our work offers a robust method for fully characterising non-Markovian noise, significantly advancing both our theo-

---

\* These authors contributed equally to this work  
christina.giar@gmail.com  
tyler.jones@fiasqo.io

retical understanding and the development of noise mitigation techniques.

## II. MULTI-TIME QUANTUM PROCESS TOMOGRAPHY

Consistent with our experimental setup, we consider a scenario where a single quantum system undergoes a sequence of three operations at specified times, see Fig 1. The purpose of multi-time process tomography is to extract, from a finite set of measurements, sufficient information that allows one to predict the joint probability for any other sequence of measurements [30, 32, 33]. The mathematical object that encodes all needed information is the process matrix—also known as quantum strategy [34], comb [32], or process tensor [35]—which is a convenient representation of a quantum stochastic process [36].

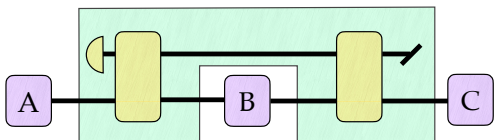


FIG. 1. A three-time quantum process involving state preparation and two gates. The bottom line is the system and the top line is the environment. The boxes  $A, B$  and  $C$  denote operations on the system at three different times.

Let us label  $A, B$ , and  $C$  the times at which the operations take place. In Figure 1, the bottom line is the system and the top line is the environment. The operations are represented by general completely positive (CP), trace-non-increasing maps from an input to an output Hilbert space so that, for example at time  $A$ , the joint input-output space is  $\mathcal{H}^A = \mathcal{H}^{A_I} \otimes \mathcal{H}^{A_O}$ . The map can be expressed in Choi form [37, 38] (see Supplementary Material) as an operator  $M_{a|x}^A \in \mathcal{L}(\mathcal{H}^A)$ ,  $M_{a|x}^A \geq 0$ , where  $a$  denotes the measurement outcome,  $x$  denotes the setting (i.e., the choice of operation), and  $\mathcal{L}(\mathcal{H})$  the space of linear operators over  $\mathcal{H}$  [39]. For each setting choice  $x$ , a complete set of outcomes defines an instrument [40], expressed as a set  $\{M_{a|x}^A\}_a$  such that  $\sum_a \text{Tr}_{A_O} M_{a|x}^A = \mathbb{1}^{A_I}$ . The process matrix is an operator on the joint space of all inputs and outputs,  $W^{ABC} \in \mathcal{L}(\mathcal{H}^A \otimes \mathcal{H}^B \otimes \mathcal{H}^C)$ ,  $W^{ABC} \geq 0$ , which allows one to calculate arbitrary joint probabilities for a sequence of outcomes  $a, b, c$ , given settings  $x, y, z$ , through the generalised Born rule [41]

$$p(a, b, c | x, y, z) = \text{Tr}[W^{ABC}(M_{a|x}^A \otimes M_{b|y}^B \otimes M_{c|z}^C)]. \quad (1)$$

Formally, we can regard  $W^{ABC}$  as a “density operator over time”, where each time instant corresponds to a pair of subsystems, an input and an output space. As output spaces encode the causal influence from an operation to future ones, the final output space can always

be discarded (hence, the final time  $C$  has only an input space). Furthermore in our scenario the first operation is a strong state preparation, which decorrelates the system from the environment allowing us to discard the first input space  $A_I$ . Thus for our experiment the process matrix is  $W^{ABC} \equiv W^{A_O B_I B_O C_I}$ .

One can reconstruct the process matrix using similar techniques as for ordinary state tomography, namely one can invert Eq. (1) and write  $W$  as a function of the probabilities. A convenient choice for the instruments is projective measurements  $\{\Pi_{a|x}\}_a$  immediately followed by the preparation of a state  $\rho_x$ , which correspond to operations of the form  $M_{a|x}^A = \Pi_{a|x}^{A_I} \otimes \rho_x^{A_O}$ , where  $A_O^T$  denotes transposition on system  $A_O$  and reflects our choice of convention, consistent with Eq. (1).

## III. MULTI-TIME TOMOGRAPHY PROTOCOL ON A SUPERCONDUCTING QUBIT

The experiment was conducted separately on two sets of superconducting hardware; an in-house processor at the University of Queensland, which will be referred to as `uq`, and a cloud processor from IBM Quantum with the moniker `ibm_perth`.

The experiment conducted on the `uq` processor used two capacitively-coupled flux-tunable transmons on a 5-qubit chip, mounted in a dilution refrigerator with a base temperature of around 15 mK. Each qubit is coupled to a dedicated resonator for readout. Flux lines are used in conjunction with a magnetic coil fixed to the chip to control transition frequencies, providing a degree of freedom by which qubit-qubit interaction strengths can be controlled.

The experiments on the `ibm_perth` processor addressed a single qubit on an 8-qubit chip. In both experiments, the system of interest is a single qubit chosen to be a corner qubit on the chip such that its closest environment is a single nearby qubit, a case that is studied with model simulations in the Appendix. In general, though, all the other qubits are part of the environment which also comprises any other degrees of freedom interacting with the system, as well as classical sources of noise.

To implement the three-time process tomography, we set the Pauli operators as our observables  $\mathcal{M} = \{X, Y, Z\}$  and their eigenstates as the input states  $\mathcal{B} = \{X_+, X_-, Y_+, Y_-, Z_+, Z_-\}$ . These form a tomographically (over) complete basis. We also define a set of operations within a basis gate set  $\mathcal{G} = \{I, R_X(\pi/2), R_X(-\pi/2), R_Y(\pi/2), R_Y(-\pi/2), R_X(\pi)\}$ . These operations are, by necessity, sufficient to prepare and measure all combinations of basis states and observables. Multi-time process tomography consists of temporally stacking two traditional process tomography protocols, forming a (prepare  $\rightarrow$  process  $\rightarrow$  measure  $\rightarrow$  prepare  $\rightarrow$  process  $\rightarrow$  measure) protocol, where preparations are on spaces  $A_O, B_O$ , while measurements

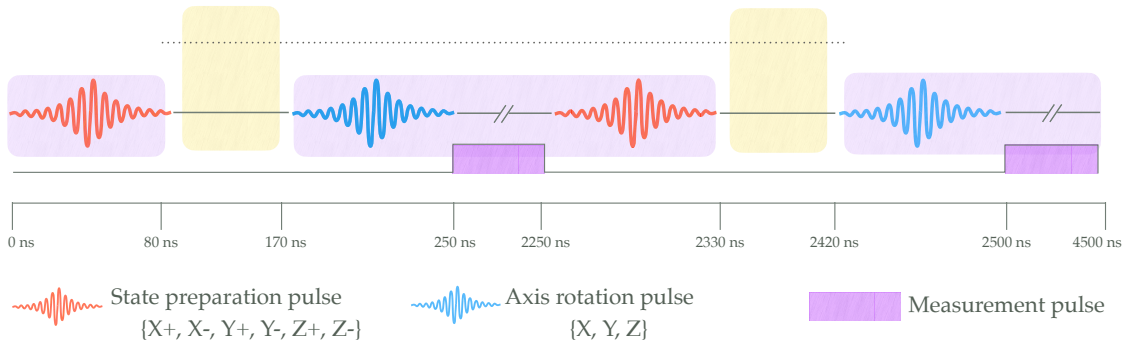


FIG. 2. A visualisation of the pulse protocol for the tomography data. The solid and dotted line is the system and environment respectively, and the two yellow boxes are the system-environment interaction.

are on  $B_I, C_I$ . In these experiments, no operation is performed between each preparation and the subsequent measurement, so the process is composed of two identity channels from  $A_O$  to  $B_I$  and from  $B_O$  to  $C_I$ . Hence, by ‘process’ in the above protocol, we mean that for times  $t_1$  and  $t_2$  the system freely evolves and so the ideal channels realised should be the identity channels. Tomography aims to characterise departures from this idealisation, representing noise in the process due to a system-environment interaction during the free evolution. The preparation states are drawn from  $\mathcal{B}$  and measurement observables from  $\mathcal{M}$ , resulting in  $|\mathcal{B}|^2|\mathcal{M}|^2 = 324$  unique protocols. The general form of this protocol is illustrated in Fig. 2. Together with Fig. 1, we can see the multi-time quantum process and the times when we make the operations to gather the data. Note that the system can in principle interact with its environment at any time, i.e., during the tomography operations too. The tomography protocol assumes that this is not the case and it is an intrinsic weakness of the presented protocol. New developments on this tomography approach claim to have circumvented this potential issue [42].

To begin, all qubits were initialised in the ground state through a standard long wait-time routine. This is a deterministic operation and ensures that both system and environment are decorrelated. The system qubit is then prepared into some basis state  $b_0 \in \mathcal{B}$  using the appropriate rotation  $p_0 \in \mathcal{G}$ . This occurs at  $A$ . The system and environment are then left to freely evolve for time  $t_1$ .

At  $B$  we apply a projective measurement of the observable  $m_0 \in \mathcal{M}$  on the system qubit, consisting of some rotation gate  $r_0 \in \mathcal{G}$  to facilitate measurement of the correct axis, followed by a readout signal. The reflected readout signal is then classified as 0 or 1 and the result is stored in memory. After the mid-circuit measurement, another rotation  $p_1 \in \mathcal{G}$  is applied to prepare a new qubit state. Conditional on the eigenstate collapse in the mid-circuit measurement, this operation prepares the system qubit into one of the basis states  $b_1, \tilde{b}_1 \in \mathcal{B}$ . For example, if a protocol measures  $m_0 = X$  and applies rotation  $p_1 = I$ , the prepared state is either  $b_1 = X_+$  or  $\tilde{b}_1 = X_-$ .

The actual prepared state is then identified by checking the result of the mid-circuit measurement. In this way, we can obtain a complete set of preparations over all experimental runs without the need for each prepared state to be chosen deterministically. This simple but critical post-processing technique is designed to avoid the need for dynamic, fast feed-forward control, which would otherwise be required for conditional operations. Following these operations, the system and environment are left to freely evolve for time  $t_2$ . In this protocol, we chose  $t_1$  and  $t_2$  according to our simulations (see Supplemental Material). Assuming one more qubit as the environment, the given experimental parameters of each qubits resonance frequency, their interaction parameter and their Hamiltonian, we obtained several pairs of  $(t_1, t_2)$  that maximise non-Markovianity of the process.

Finally, at  $C$  we measure our second observable  $m_1 \in \mathcal{M}$ . In all, the protocol is repeated  $2^{14}$  times for each of 324 prepare-measure-prepare-measure permutations, resulting in approximately  $5.3 \times 10^6$  individual shots per process characterisation experiment (one on `uq` and nine at `ibm_perth`). This data is shaped into the number of realised counts we obtain for each permutation. An example is  $(X_+, X_-, Y_+, Z_-)$  denoting that at  $A$  we prepare the state  $X_+$ , at  $B$  we projectively measure  $X_-$  and then re-prepare  $Y_+$ , and at  $C$  we projectively measure  $Z_-$ .

After obtaining the data, we are ready to calculate the experimental process matrix. A process matrix can be written in the Pauli basis,  $W = \sum_{i,j,k,l} \alpha_{i,j,k,l} \sigma_i \otimes \sigma_j \otimes \sigma_k \otimes \sigma_l$ , where  $(i,j,k,l) = [0,3]$  denotes the Pauli basis  $\mathbb{1}, \sigma_x, \sigma_y, \sigma_z$ . From Eq. 1, we see that if we apply Pauli operations at  $A, B, C$ , their expectation values will be the coefficients  $\langle \sigma_i, \sigma_j, \sigma_k, \sigma_l \rangle = \alpha_{i,j,k,l}$ . Hence, we can reconstruct the experimental process matrix, by calculating the expectation values of the sigma terms from the experimental data

$$W_{exp} = \frac{1}{16} \sum_{i,j,k,l} \langle \sigma_i, \sigma_j, \sigma_k, \sigma_l \rangle \sigma_i \otimes \sigma_j \otimes \sigma_k \otimes \sigma_l. \quad (2)$$

$W_{exp}$  is the process matrix we construct from the experimental data, but it typically does not represent a physical

one (it might be non-positive, or fail the process matrix constraints). This is typically the case for quantum state tomography too and various methods are used to obtain the physical state from the experimental one, such as maximum likelihood estimation. To obtain a physical process,  $W_{phys}$ , we use SemiDefinite Programming (SDP), where we find a positive matrix that minimises its distance (we used Frobenius distance) with the  $W_{exp}$ . The SDP is the following:

$$\begin{aligned} & \text{variable } W_{phys} \text{ Hermitian Semidefinite} \\ & \text{minimize Frobenius Norm}(W_{exp} - W_{phys}) \quad (3) \\ & \text{subject to } L_V(W_{phys}) == W_{phys} \\ & \quad \text{Tr}(W_{phys}) == 4, \end{aligned}$$

where  $L_V$  is an operator that projects a matrix to the space of valid process matrices [43] and the normalisation constraint helps the SDP to bound the solution. Using the  $W_{phys}$  we report in the Results section our findings on tomography and non-Markovianity.

Our tomography protocol differs from related works in that we implement full multi-time process tomography by reconstructing the full process matrix. Concretely, Xiang *et al.* implement projective mid-circuit measurements but limit their analysis to an under-complete set of POVMs to construct a ‘restricted’ process matrix [28]. Similarly, White *et al.* restrict their tomography to only sequences of unitary operations and final measurement, with reference to the difficulty of mid-circuit measurement in superconducting processors [30]. Related work by the same authors extends their analysis to non-unital maps by introducing an ancillary qubit and entangling operations, obtaining a separate class of restricted information known as classical shadows [29]. Obtaining the full process matrix provides the first complete characterisation of non-Markovian noise, which underpins the novelty of our method and findings.

#### IV. RESULTS: TOMOGRAPHY AND NON-MARKOVIAN NOISE

Figure 3 provides insight into the qualitative differences between two experimental (physical) process matrices,  $W_{phys}$ , using data from the in-house `uq` processor and from the `ibm_perth` processor. The process matrix from `ibm_perth` is visually almost indistinguishable from a noiseless (or Markovian) process with identity channels between the times  $A$ ,  $B$  and  $C$ , while the `uq` process maintains the qualitative structure of the identity channels with evident noise.

Overall, we took tomographic data for one process on the `uq` processor and nine on `ibm_perth` with varying  $t_1$  and  $t_2$ . Variations in free evolution times were explored after simulating each system with a simple one-qubit environment model and finding that both general and quantum non-Markovianity depend highly on these times, with a particular structure (see Supplementary

Material). While we chose the experimental  $t_1, t_2$  that maximise non-Markovianity in the simulation, no such structure was observed in the experiments we conducted.

Given the physical process matrices for each of the ten processes characterised (broadly denoted as  $W_{phys}$ ), we aim to detect and quantify non-Markovianity. To this end, we calculate a measure of distance of each  $W_{phys}$  with its closest Markovian process matrix  $W_M$ . We construct  $W_M$  by discarding temporal correlations, combining the two channels [30, 44]

$$W_M = T_1^{A \circ B_I} \otimes T_2^{B \circ C_I}, \quad (4)$$

where  $T_1^{A \circ B_I} = \text{Tr}_{B \circ C_I} W_{phys}$  and  $T_2^{B \circ C_I} = \text{Tr}_{A \circ B_I} W_{phys}$ . As a measure of distance, we consider the Jensen-Shannon divergence (JSD) for two matrices  $W_1$  and  $W_2$ :

$$JSD(W_1, W_2) = H\left(\frac{W_1 + W_2}{2}\right) - \frac{1}{2}(H(W_1) + H(W_2)), \quad (5)$$

where  $H(W) = -\text{Tr} W \log W$  is the von Neumann entropy. The square root of the JSD operates as a distance measure between states or channels, and has utility in particular for quantifying non-Markovian dynamics [45]. The results for  $\sqrt{JSD}$  across the ten processes are reported in Table I. These indicate that non-Markovian effects were significant in both platforms for all choices of parameters, but were more pernicious on the `uq` processor. This is consistent with the appreciably stronger idle qubit-qubit interaction on this chip.

Evolution	General	Quantum
$(t_1, t_2)$ ns	$\sqrt{JSD} \times 10^{-1}$	$\mathcal{N} \times 10^{-2}$
(97, 97)	$5.04 \pm 0.07$	$8.66 \pm 0.86$
(21, 21)	$1.77 \pm 0.17$	$1.61 \pm 0.58$
(21, 24)	$1.64 \pm 0.17$	$1.66 \pm 0.61$
(21, 28)	$1.81 \pm 0.15$	$2.22 \pm 0.69$
(24, 21)	$1.60 \pm 0.16$	$1.94 \pm 0.64$
(24, 24)	$1.85 \pm 0.18$	$1.71 \pm 0.65$
(24, 28)	$2.06 \pm 0.14$	$2.44 \pm 0.68$
(28, 21)	$1.96 \pm 0.15$	$2.00 \pm 0.71$
(28, 24)	$1.85 \pm 0.14$	$2.04 \pm 0.67$
(28, 28)	$1.76 \pm 0.17$	$1.83 \pm 0.62$

TABLE I. The square root Jensen-Shannon divergence ( $\sqrt{JSD}$ ) and negativity ( $\mathcal{N}$ ) of the multi-time process matrices reconstructed for each processor. Each experiment has two periods of free evolution, which are denoted by  $t_1$  and  $t_2$ , shown in nanoseconds. The first row shows the `uq` data and the next nine runs were from `ibm_perth`.

A natural subsequent inquiry is whether non-Markovianity originates from a quantum source; the value of distinguishing between classical or quantum environments lies in the manifestly different dynamics they induce [46–49]. The quantum nature of non-Markovianity in the process is captured by quantum correlations across the evolution from  $A$  to  $B$  and from  $B$

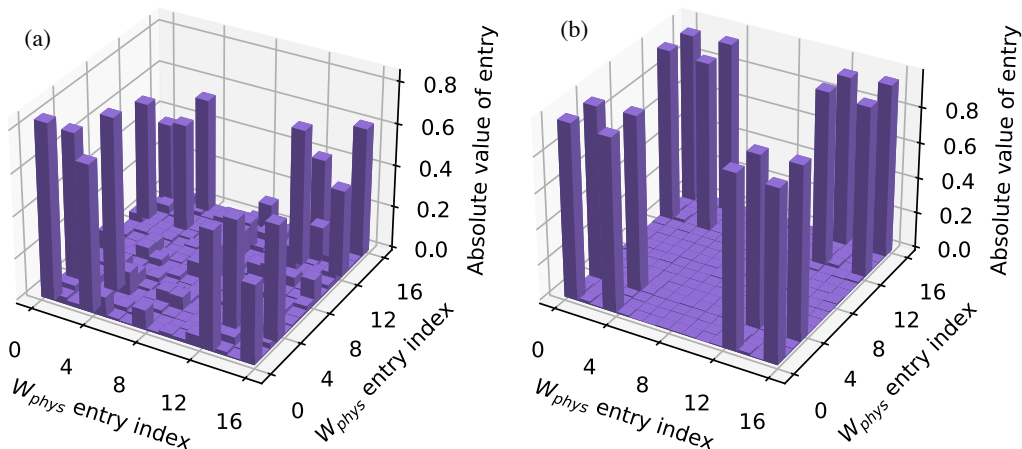


FIG. 3. A visualisation of the absolute valued entries ( $z$  axis) of the full  $16 \times 16$  multi-time process matrix ( $x$  and  $y$  axis are running across the 2 dimensions of the matrix), constructed with tomographic data from (a) the `uq` processor and (b) the `ibm_perth` processor.

to  $C$ . This maps to entanglement across the bipartition  $A_O B_I | B_O C_I$  in the four-qubit state representation of the process,  $\rho^{A_O B_I | B_O C_I} := \frac{W^{ABC}}{\text{Tr} W^{ABC}}$ . To measure entanglement, we take the computationally inexpensive metric of negativity,

$$\mathcal{N}(\rho) = \left| \sum_{\lambda_i < 0} \lambda_i \right| = \sum_i \frac{|\lambda_i| - \lambda_i}{2}, \quad (6)$$

where  $\rho = \rho^{(A_O B_I)^T | B_O C_I}$ , where  $T$  denotes partial transposition (it can be on either of the two subsystems,  $A_O B_I$  or  $B_O C_I$ ), and  $\lambda_i$  are the eigenvalues of  $\rho$  [50].

Quantum multi-time correlations are observed on each processor, but are markedly enhanced on the `uq` processor. This is consistent with the increased interaction strength observed between the system qubit and its primary interacting ‘memory’ qubit on the `uq` processor. The negativities reported over the nine `ibm_perth` runs all lay within each others’ credible intervals, indicating that the quantum non-Markovianity present in each process was effectively invariant across the  $(t_1, t_2)$  landscape explored. In all measurements, the reported uncertainty denotes 95% credible intervals determined by bootstrapping techniques as described in Supplementary Material, accounting for sampling noise.

Using the natural log in Eq. 5, the  $\sqrt{JSD}$  metric is bounded between 0 and  $\ln 2$  [51], lending scale to the magnitude of our findings which lie on the order of  $10^{-1}$ . This is a strong signal that the multi-time processes characterised on each device are easily distinguishable from the most likely temporally uncorrelated candidates. Negativity serves as an entanglement monotone and is therefore bounded from below by zero (completely separable) [50]. In state space, negativity is upper bounded by the maximally entangled state ( $\frac{3}{2}$  for four qubits), roughly two orders of magnitude larger than in our mea-

surements. This state does not correspond to a valid process matrix (because the space of states is larger than that of process matrices) but provides a sense of scale for the results reported.

In summary, we observe and quantify non-Markovian dynamics and quantum correlations with high confidence on both `uq` and `ibm_perth` processors, highlighting the relevance of correlated noise in the design of future mitigation techniques. Our results demonstrate the practicality of our methods for characterising this noise.

## V. CONCLUSION

We report the first experimental full characterisation of a multi-time quantum process on a superconducting qubit. We implement ten three-time processes using an in-house superconducting processor and a cloud processor from IBM Quantum. We characterise the processes using the process matrix formalism and provide a measure of their non-Markovian noise; both general and stemming from quantum correlations across time. We find that non-Markovian noise is present in all cases, with a significant proportion originating from genuine quantum correlations. A comparison with a simple system-environment model indicates that the influence of nearest-neighbour qubits is not sufficient to account for all the observed quantum non-Markovianity. Our results demonstrate the capacity of our methods to fully describe multi-time processes and confidently measure and characterise non-Markovian noise, laying the foundation for novel error-mitigation techniques set to impact current and future quantum devices.

## ACKNOWLEDGMENTS

We thank Xin He for providing support in preparing the tomography experiments on the uq processor, and Gerardo Paz Silva for sharing relevant literature. We acknowledge the use of IBM Quantum services for this work. The views expressed are those of the authors and do not reflect the official policy or position of IBM or the IBM Quantum team. CG acknowledges funding from the Sydney Quantum Academy Fellowship and the UTS Chancellor’s Research Fellowship. FC was supported

by the Wallenberg Initiative on Networks and Quantum Information (WINQ). This work was supported by the Australian Research Council (ARC) Centre of Excellence for Quantum Engineered Systems grant (CE 170100009). Nordita is supported in part by NordForsk. Finally, we acknowledge the traditional owners of the land on which the University of Queensland, the University of Technology Sydney, and Macquarie University are situated, the Turrbal and Jagera people, the Gadigal people of the Eora Nation, and Wallumattagal clan of the Dharug Nation.

- 
- [1] J. Morris, F. A. Pollock, and K. Modi, Quantifying non-markovian memory in a superconducting quantum computer, *Open Systems & Information Dynamics* **29**, [10.1142/S123016122250007X](https://doi.org/10.1142/S123016122250007X) (2022).
- [2] M. McEwen *et al.*, Removing leakage-induced correlated errors in superconducting quantum error correction, *Nature Communications* **12**, [10.1038/s41467-021-21982-y](https://doi.org/10.1038/s41467-021-21982-y) (2021).
- [3] K. Young, S. Bartlett, R. J. Blume-Kohout, J. K. Gamble, D. Lobser, P. Maunz, E. Nielsen, T. J. Proctor, M. Revella, and K. M. Rudinger, *Diagnosing and Destroying Non-Markovian Noise*, Tech. Rep. (United States, 2020).
- [4] J. Piilo, S. Maniscalco, K. Härkönen, and K.-A. Suominen, Non-markovian quantum jumps, *Phys. Rev. Lett.* **100**, 180402 (2008).
- [5] H.-P. Breuer, E.-M. Laine, and J. Piilo, Measure for the degree of non-markovian behavior of quantum processes in open systems, *Phys. Rev. Lett.* **103**, 210401 (2009).
- [6] A. Rivas, S. F. Huelga, and M. B. Plenio, Entanglement and non-markovianity of quantum evolutions, *Phys. Rev. Lett.* **105**, 050403 (2010).
- [7] Á. Rivas, S. F. Huelga, and M. B. Plenio, Quantum non-markovianity: characterization, quantification and detection, *Rep. Prog. Phys.* **77**, 094001 (2014).
- [8] H.-P. Breuer, E.-M. Laine, J. Piilo, and B. Vacchini, Colloquium: Non-markovian dynamics in open quantum systems, *Rev. Mod. Phys.* **88**, 021002 (2016).
- [9] D. Chruściński, A. Kossakowski, and A. Rivas, Measures of non-markovianity: Divisibility versus backflow of information, *Phys. Rev. A* **83**, 052128 (2011).
- [10] I. de Vega and D. Alonso, Dynamics of non-markovian open quantum systems, *Reviews of Modern Physics* **89**, 015001 (2017).
- [11] K. Takeda *et al.*, Optimized electrical control of a si/sige spin qubit in the presence of an induced frequency shift, *npj Quantum Information* **4**, 54 (2018).
- [12] S. Freer *et al.*, A single-atom quantum memory in silicon, *Quantum Science and Technology* **2**, 015009 (2017).
- [13] R. Savytsky *et al.*, An electrically driven single-atom “flip-flop” qubit, *Science Advances* **9**, eadd9408 (2023).
- [14] A. M. J. Zwerver *et al.*, Qubits made by advanced semiconductor manufacturing, *Nature Electronics* **5**, 184 (2022).
- [15] S. G. J. Philips *et al.*, Universal control of a six-qubit quantum processor in silicon, *Nature* **609**, 919 (2022).
- [16] O. Oreshkov, F. Costa, and Č. Brukner, Quantum correlations with no causal order, *Nat. Commun.* **3**, 1092 (2012).
- [17] O. Oreshkov and C. Giarmatzi, Causal and causally separable processes, *New J. Phys.* **18**, 093020 (2016).
- [18] C. Giarmatzi and F. Costa, Witnessing quantum memory in non-Markovian processes, *Quantum* **5**, 440 (2021).
- [19] S. Shrapnel, F. Costa, and G. Milburn, Quantum markovianity as a supervised learning task, *International Journal of Quantum Information* **16**, 1840010 (2018).
- [20] P. Taranto, F. A. Pollock, and K. Modi, Non-markovian memory strength bounds quantum process recoverability, *npj Quantum Information* **7**, 149 (2021).
- [21] G. E. Fux, E. P. Butler, P. R. Eastham, B. W. Lovett, and J. Keeling, Efficient exploration of hamiltonian parameter space for optimal control of non-markovian open quantum systems, *Phys. Rev. Lett.* **126**, 200401 (2021).
- [22] P. Figueroa-Romero, K. Modi, R. J. Harris, T. M. Stace, and M.-H. Hsieh, Randomized benchmarking for non-markovian noise, *PRX Quantum* **2**, 040351 (2021).
- [23] J. Morris, F. A. Pollock, and K. Modi, *Quantifying non-markovian memory in a superconducting quantum computer*.
- [24] S. Milz, F. A. Pollock, and K. Modi, Reconstructing non-markovian quantum dynamics with limited control, *Phys. Rev. A* **98**, 012108 (2018).
- [25] R. N. Muñoz, L. Frazer, G. Yuan, P. Mulvaney, F. A. Pollock, and K. Modi, Memory in quantum dot blinking, *Phys. Rev. E* **106**, 014127 (2022).
- [26] K. Goswami, C. Giarmatzi, C. Monterola, S. Shrapnel, J. Romero, and F. Costa, Experimental characterization of a non-markovian quantum process, *Phys. Rev. A* **104**, 022432 (2021).
- [27] G. A. L. White, C. D. Hill, F. A. Pollock, L. C. L. Hollenberg, and K. Modi, Demonstration of non-markovian process characterisation and control on a quantum processor, *Nature Communications* **11**, [10.1038/s41467-020-20113-3](https://doi.org/10.1038/s41467-020-20113-3) (2020).
- [28] L. Xiang *et al.*, *Quantify the non-markovian process with intervening projections in a superconducting processor* (2021), [arXiv:2105.03333](https://arxiv.org/abs/2105.03333).
- [29] G. A. L. White, F. A. Pollock, L. C. L. Hollenberg, C. D. Hill, and K. Modi, *From many-body to many-time physics* (2021), [arXiv:2107.13934](https://arxiv.org/abs/2107.13934).
- [30] G. White, F. Pollock, L. Hollenberg, K. Modi, and C. Hill, Non-markovian quantum process tomography, *PRX Quantum* **3**, [10.1103/prxquantum.3.020344](https://doi.org/10.1103/prxquantum.3.020344) (2022).
- [31] IBM Quantum, (2023).

- [32] G. Chiribella, G. M. D’Ariano, and P. Perinotti, Theoretical framework for quantum networks, *Phys. Rev. A* **80**, 022339 (2009), arXiv:0904.4483 [quant-ph].
- [33] F. Costa and S. Shrapnel, Quantum causal modelling, *New J. Phys.* **18**, 063032 (2016).
- [34] G. Gutoski and J. Watrous, Toward a general theory of quantum games, in *In Proceedings of 39th ACM STOC* (2006) pp. 565–574, quant-ph/0611234.
- [35] F. A. Pollock, C. Rodríguez-Rosario, T. Frauenheim, M. Paternostro, and K. Modi, Non-markovian quantum processes: Complete framework and efficient characterization, *Physical Review A* **97**, 012127 (2018).
- [36] G. Lindblad, Non-markovian quantum stochastic processes and their entropy, *Comm. Math. Phys.* **65**, 281 (1979).
- [37] A. Jamiolkowski, Linear transformations which preserve trace and positive semidefiniteness of operators, *Rep. Math. Phys.* **3**, 275 (1972).
- [38] M.-D. Choi, Completely positive linear maps on complex matrices, *Linear Algebra and its Applications* **10**, 285 (1975).
- [39] T. Heinosaari and M. Ziman, *The Mathematical Language of Quantum Theory: From Uncertainty to Entanglement* (Cambridge University Press, 2011).
- [40] E. B. Davies and J. T. Lewis, An operational approach to quantum probability, *Communications in Mathematical Physics* **17**, 239 (1970).
- [41] S. Shrapnel, F. Costa, and G. Milburn, Updating the born rule, *New Journal of Physics* **20**, 053010 (2018).
- [42] G. A. L. White, P. Jurcevic, C. D. Hill, and K. Modi, Unifying non-markovian characterisation with an efficient and self-consistent framework (2023), arXiv:2312.08454.
- [43] M. Araújo, C. Branciard, F. Costa, A. Feix, C. Giarmatzi, and Č. Brukner, Witnessing causal nonseparability, *New J. Phys.* **17**, 102001 (2015).
- [44] C. Giarmatzi and F. Costa, A quantum causal discovery algorithm, *npj Quantum Information* **4**, 17 (2018).
- [45] F. Settimo, H.-P. Breuer, and B. Vacchini, Entropic and trace-distance-based measures of non-markovianity, *Physical Review A* **106**, 10.1103/physreva.106.042212 (2022).
- [46] P. Jouzdani and E. R. Mucciolo, Numerical evaluation of the fidelity error threshold for the surface code, *Phys. Rev. A* **90**, 012315 (2014).
- [47] G. A. Paz-Silva, L. M. Norris, and L. Viola, Multiqubit spectroscopy of gaussian quantum noise, *Physical Review A* **95**, 10.1103/physreva.95.022121 (2017).
- [48] F. Beaudoin, L. M. Norris, and L. Viola, Ramsey interferometry in correlated quantum noise environments, *Phys. Rev. A* **98**, 020102 (2018).
- [49] G. A. Paz-Silva, L. M. Norris, F. Beaudoin, and L. Viola, Extending comb-based spectral estimation to multiaxis quantum noise, *Physical Review A* **100**, 10.1103/physreva.100.042334 (2019).
- [50] G. Vidal and R. F. Werner, Computable measure of entanglement, *Physical Review A* **65**, 10.1103/physreva.65.032314 (2002).
- [51] J. Lin, Divergence measures based on the shannon entropy, *IEEE Transactions on Information Theory* **37**, 145 (1991).

## Appendix A: Device characteristics, errors and simulation

### Experimental devices

The primary device used was a superconducting quantum processor consisting of five flux-tunable transmons, fabricated by Quantware [1]. System characteristics of the transmon we performed multi-time tomography on (‘System’) and the dominant interacting transmon (‘Memory’) are provided in Table II. These characteristics include T1 and T2, the relaxation and dephasing lifetimes. The ‘System’ qubit only has one nearest-neighbour coupling to the ‘Memory’ qubit, which in turn is coupled to two other qubits. Charge lines and flux lines to each qubit permit XY control and frequency tunability respectively. A common feedline couples to individual dedicated resonators for each transmon qubit. Typical gate fidelities on this device are 99.5%, while readout fidelity is around 93%.

The custom-built open-source library `sqdtoolz` [2] is used to orchestrate the array of high-precision instruments required to execute control protocols on our quantum processor. This includes the synchronised generation and timing of microwave-frequency pulsed signals for control and measurement, a continuous microwave-frequency pump signal for parametric amplifier operation and a stable DC signal for frequency tuning purposes.

Characteristic	System qubit	Memory qubit
Symmetry point frequency	5.97 GHz	5.03 GHz
Operational frequency ( $\omega$ )	5.11 GHz	5.03 GHz
Coupling to system ( $g_{12}$ )	N/A	11 MHz
Relaxation time	14 $\mu$ s	10 $\mu$ s
Dephasing time	1.8 $\mu$ s	6 $\mu$ s

TABLE II. The characteristics of the major interacting transmon qubits in the experimental processor. The system qubit is operating at a transition frequency far from its symmetry point, which increases its sensitivity to flux noise and in turn reduces T2.

Experiments are also performed on the cloud 7-qubit quantum processor `ibm_perth`, as provided by IBM Quantum [3]. This system offers increased coherence times and gate fidelities at the expense of frequency control. Transmon characteristics can be found in Table III. Gate fidelities are reported at 99.95%, and readout fidelity at 97.5%.

### Error estimation

The credible intervals reported in Table 1 in the main text, were calculated using the non-parametric resam-

Characteristic	System qubit	Memory qubit
Qubit frequency ( $\omega$ )	5.16 GHz	4.98 GHz
Coupling to system ( $g_{12}$ )	N/A	3 MHz
Relaxation time	207 $\mu$ s	102 $\mu$ s
Dephasing time	295 $\mu$ s	113 $\mu$ s

TABLE III. The characteristics of the major interacting transmon qubits in the IBM cloud processor. For this system, we have no control over frequency and therefore no control over interaction strength.

pling technique of bootstrapping. Bootstrapping a standard deviation for some metric  $\hat{\theta}(\hat{X})$  relies on the assumption that the relative frequency of the measured  $\hat{X}$  is representative of the underlying distribution which  $\hat{X}$  is drawn from. In our case,  $\hat{X}$  is a measured set of shot probabilities, which may look something like  $\{00: 0.7773, 10: 0.1738, 01: 0.0421, 11: 0.0068\}$ , where, 00 for example corresponds to the probability of getting the plus state in both measurements at  $B$  and  $C$ . We resample 8000 shots from a multinomial distribution with these underlying relative frequencies, over 1000 trials, creating a set of bootstrapped results  $\hat{X}_i$ . The simulated distribution of the metric of interest is then evaluated as  $\hat{\theta}(\hat{X}_i)$  and twice the standard deviation of this distribution is used to calculate the 95% credible interval of the reported metric  $\hat{\theta}(\hat{X})$ . This technique is designed to account for shot noise in the finite-sample estimates of observables, and does not account for systematic error at the hardware level (gate miscalibration, readout misclassification). Finally, we rely on bias correction in the bootstrapping process; the sample mean of the metric  $\hat{\theta}(\hat{X}_i)$  was in general not equal to the measured  $\hat{\theta}(\hat{X})$  (sometimes outside of the credible interval).

### Simulated process

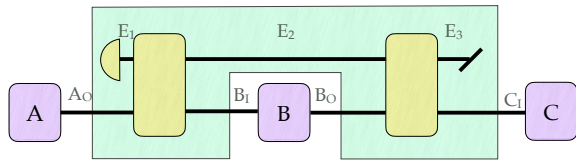


FIG. 4. A three-time quantum process involving state preparation and two gates acting on both systems.

In both platforms used, the qubit we probe belongs to a larger multi-qubit array. The particular qubits we choose each have one nearest-neighbour qubit, with which they are directly coupled, as well as additional distant qubits (two or more degrees of separation), with which interactions will be weaker. We therefore take the simplest

model of our environment to be that of the single coupled qubit, as shown in Fig. 4. This interaction can be described by the Hamiltonian [4]

$$H = \frac{\omega_1}{2}(\mathbb{1} \otimes \sigma_z) + \frac{\omega_2}{2}(\sigma_z \otimes \mathbb{1}) + g_{12}(\sigma_+ \otimes \sigma_- + \sigma_- \otimes \sigma_+), \quad (\text{A1})$$

where  $\omega_{1,2}$  are the resonance frequencies of the system and memory qubit, respectively, and  $\sigma_{+,-}$  are the creation and annihilation operators, respectively. Then the free evolution of system-memory (the environment) is expressed as  $U = e^{-iHt}$ , where  $t$  is the time of the evolution.

To write the process matrix for our system, we start with writing the terms: the initial state of the environment  $\rho^{E_1}$ , the channel  $T_1^{A_0 E_1^T B_1 E_2}$  and the second channel  $T_2^{B_0 E_2^T C_1 E_3}$  (see Fig 4), where the superscript  $T$  on a system denotes partial transposition for that system. To obtain the process matrix, we combine the terms with the link product and trace out all the environment systems

$$W = \text{Tr}_{E_1, E_2, E_3}(\rho^{E_1} * T_1^{A_0 E_1^T B_1 E_2} * T_2^{B_0 E_2^T C_1 E_3}), \quad (\text{A2})$$

where  $\rho^{E_1} = |0\rangle$  because all qubits on the chip are initialised to the ground state,  $T_1^{A_0 E_1^T B_1 E_2} = [[U]]^{A_0 E_1 B_1 E_2}$  and  $T_2^{B_0 E_2^T C_1 E_3} = [[U]]^{B_0 E_2 C_1 E_3}$ , and  $[[U]]$  is the Choi form of  $U$ , without the partial transposition.

*Choi matrix definition:* The Choi matrix  $M^{A_I A_O} \in \mathcal{L}(\mathcal{H}^{A_I} \otimes \mathcal{H}^{A_O})$ , isomorphic to a CP map  $\mathcal{M}^A : \mathcal{L}(\mathcal{H}^{A_I}) \rightarrow \mathcal{L}(\mathcal{H}^{A_O})$  is defined as  $M^{A_I A_O} := [\mathcal{I} \otimes \mathcal{M}(|\mathbb{1}\rangle\langle\mathbb{1}|)]^T$ , where  $\mathcal{I}$  is the identity map,  $|\mathbb{1}\rangle = \sum_{j=1}^{d_{A_I}} |jj\rangle \in \mathcal{H}^{A_I} \otimes \mathcal{H}^{A_I}$ ,  $\{|j\rangle\}_{j=1}^{d_{A_I}}$  is an orthonormal basis on  $\mathcal{H}^{A_I}$  and  $T$  denotes matrix transposition in that basis and some basis of  $\mathcal{H}^{A_O}$ .

*Link product definition:*  $W^{xyz} = \rho^x * T^{yz} = [(\rho^x \otimes \mathbb{1}^{yz})(\mathbb{1}^x \otimes T^{yz})]$ .

We see that the free evolution,  $U$ , depends on the parameters of the Hamiltonian,  $\omega_1$ ,  $\omega_2$ ,  $g_{1,2}$ , and the time  $t$ . Hence, our process matrix will also depend on these parameters,  $W(\omega_1, \omega_2, g_{1,2}, t_1, t_2)$ . To simulate the process on `uq`, experimental parameters were measured to be as given in Table II, and we scan  $t_1$  and  $t_2$  from 85 to 115 ns, capturing the 97 ns process conducted in the experiment. In the experiment, we chose  $t_1 = t_2 = 97$  ns because in the simulation these times maximised non-Markovianity. For the process on `ibm_perth`, the parameters were fixed at the values available in Table III, and we scan  $t_1$  and  $t_2$  between 17 and 33 ns, capturing the permutations of  $t_1 = [21.33, 24.89, 28.44]$  ns and  $t_2 = [21.33, 24.89, 28.44]$  ns conducted in the experiment, which are centered around a peak of non-Markovianity in the simulation. The `ibm_perth` process simulation yielded the results in Fig. 5. We obtained a similar structure for the `uq` process.

According to these results, the experimental runs where evolution times are  $t_1 = t_2 = 24.89$  ns should maximise both metrics of non-Markovianity on `ibm_perth`, while other settings ( $t_1 = 21.33$  ns and  $t_2 = 28.44$  ns)

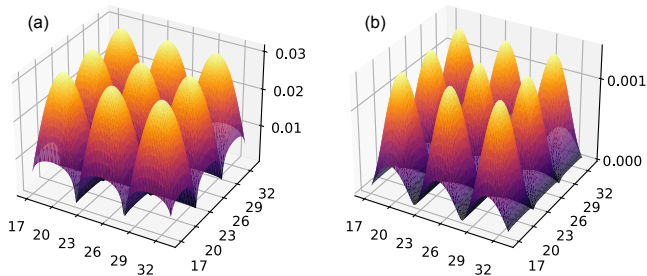


FIG. 5. Simulated (a)  $\sqrt{JSD}$  and (b)  $\mathcal{N}$  values for the `ibm_perth` processor over a range of free evolution times  $t_1$  and  $t_2$ .

		$\max(\sqrt{JSD})$	$\max(\mathcal{N})$
uq	measured	0.504	0.087
	simulated	0.270	0.091
ibm_perth	measured	0.206	0.024
	simulated	0.031	0.001

TABLE IV. The maximum values observed for the square root Jensen-Shannon divergence ( $\sqrt{JSD}$ ) and negativity ( $\mathcal{N}$ ) across the experimentally measured (across the experimental runs, see Table 1 of main text) and simulated (at the peak of a  $(t_1, t_2)$  oscillation, see Fig. 5) multi-time processes.

should be close to fully suppressing non-Markovian dynamics. In practice, both metrics were observed to be smeared across the free evolution times scanned. This is not a particularly surprising result when contrasting the simplicity of the coupled-qubit environment described in Eq. A1 to the complexity of current-day quantum hardware, including but not limited to the extra qubits on each chip.

A point of some interest is the comparison of the maximum  $\sqrt{JSD}$  and  $\mathcal{N}$  predicted in simulation (across a reasonable  $(t_1, t_2)$  range) to the values observed in the experiment. A summary of these is provided in Table IV. The qualitative structure of the simulated values matches the results presented in this work and are reasonable quantitatively on the `uq` processor. Both metrics are heavily underestimated on the `ibm_perth` processor. This is not an unusual result; the Hamiltonian presented in Eq A1 is certainly missing several terms, both characterisable (e.g. other qubits on the chip) and unknown. Hence, although the naive model is a reasonable first-order approximation, our results show that we can probe more complex dynamics than we can simulate, making our methods a powerful tool to detect non-Markovian noise.

- 
- [1] Quantware, (2023).  
 [2] P. Pakkiam, R. Beriwal, and J. Dearlove, [Sqdttools](#) (2023).  
 [3] IBM Quantum, (2023).  
 [4] A. Blais, J. Gambetta, A. Wallraff, D. I. Schuster,

S. M. Girvin, M. H. Devoret, and R. J. Schoelkopf, Quantum-information processing with circuit quantum electrodynamics, *Physical Review A* **75**, [10.1103/physreva.75.032329](#) (2007).